H^- BEAM NEUTRALIZATION MEASUREMENTS WITH A GRIDDED-ENERGY ANALYZER, A NONINTERCEPTIVE BEAM DIAGNOSTIC *

Joseph Sherman, Eric Pitcher, and Paul Allison

MS-H818, Los Alamos National Laboratory, Los Alamos, N.M. 87545

Abstract

Transport of high-perveance H^- ion beams frequently depends on space-charge neutralization by a background plasma to reduce or eliminate space-charge defocusing. We have developed a four-grid energy analyzer (FGA) that measures the energy distributions of particles emitted radially from the beam-generated plasma. H^- beams of 80- to 90- mA current at 21-keV beam energy (which yields a −400 V potential drop for an unneutralized beam) have been studied in a 55-cm drift region using He and Xe neutralizing gases. At a sufficiently high gas density, ion energy distribution analyses show a several volt positive potential drop across the H^- beam, supporting the gas focusing concept of overneutralized H^- ion beams. There is a neutralizing gas density threshold below which no radially flowing positive ion current is observed. At low gas density, the FGA electron current is noisy (indicating the plasma is unstable) and the measured electron distributions are consistent with an underneutralized beam. With the addition of neutralizing gas, the electron current oscillations and energies decrease.

Introduction

Beam-plasma interactions observed in transport of 20-kV H^- beams[1] with current densities of approximately 50 mA/cm^2 have resulted in beam-emittance growth and consequent transport difficulties.[2] Increasing the background neutralization gas density has reduced or eliminated H^- beam emittance growth.[2,3] Time-dependent numerical modeling of beam transport in a gas has also shown this result.[4] An attempt to quantify the beam-plasma potential was made by using the emissive probe technique, but interception of the primary beam by the probe perturbed the measurement, especially at low neutralizing gas density.[3] We thus embarked on the development of the FGA that detects particles emitted radially from the beam plasma and does not intercept the primary beam. Plasma properties are then inferred from the radially flowing ions and electrons and their energy distributions.

Experiment

The energy analyzer is composed of four electrically isolated grids separated by 5-mm gaps (see insert on Fig. 1). The first grid is at wall potential and has 70% transparency with grid spacing $D = 0.08$ mm. Grid 2 potential is set to accelerate positive ions while rejecting electrons or vice versa. A 90% transparent grid 2 with $D = 0.35$ mm was chosen to minimize secondary production. Particle energy discrimination is done at grid 3, and because the voltage difference between the edge and center of a grid hole is

$$\Delta V \approx \frac{D}{2\pi}(E_2 - E_3)\,, \tag{1}$$

where E_2 = electric field in gap 2 and E_3 = electric field in gap 3, 70% transparent material was chosen to minimize this effect.[5] For typical grid 2 and 4 voltage settings, an energy spread of 0.2 eV may be expected. Grid 4 reaccelerates the analyzed particle to the FGA Faraday cup, which is biased to trap secondary electrons. A 90% transparent grid is used in this location, which gives a total analyzer transparency $T = 40\%$. The FGA entrance aperture radius is $r_a = 4$ mm, and is located $d = 6.2$ cm from the beam axis. The ion-optical effects on the analyzer resolution were considered in detail, but the most important consideration in obtaining reproducible energy resolution and calibration was the necessity to maintain the FGA at $\gtrsim 350\,^\circ$C to reduce effects of insulating layers that build up on the grids under particle impingement.[6]

Data acquisition is accomplished by digitizing the FGA current $i_{\rm FGA}$ at a constant grid 3 voltage V_3 as a function of time, typically taking 200–100 samples at 0.5- to 1.0- μs time steps. The grid 3 voltage is stepped over the range from maximum Faraday cup current to zero current, thus constructing the $i_{\rm FGA}$ versus V_3 characteristic. The FGA current then follows the relation

$$i_{\rm FGA}(V_3) \propto \int_{|eV_3|}^{\infty} f(E)dE, \qquad f(E) \propto \frac{di_{\rm FGA}}{dV_3}. \tag{2}$$

The charged particle energy distribution function $f(E)$ is then obtained by numerical differentiation of Eq. (2). An example of the electron distribution function obtained for a 30-eV electron beam accelerated from a hot filament is shown in Fig. 2. Experimentally the system is capable of 1-eV energy resolution and calibration, and has 50-nA current detection limit at 1-MHz bandwidth (BW). Finite voltage step size, detector acceptance angle, ion-optical, and wire-temperature effects can account for the 1-eV resolution noted in Fig. 2.

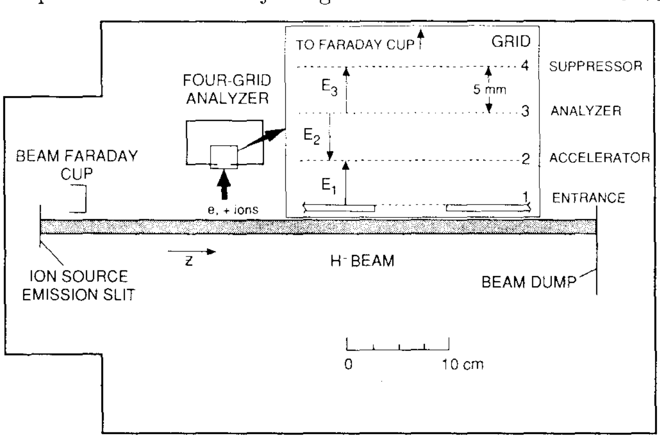

Fig. 1. Experimental setup for the beam transport and FGA schematic.

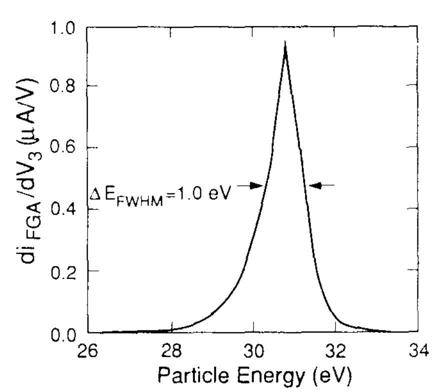

Fig. 2. Distribution function derived from our apparatus for a 30-eV electron beam. Note the offset energy scale.

The H^- ion source is a Penning surface plasma source[2] with a small (7°) angular bend (the small-angle source, SAS). This source was equipped with a slit (0.8 × 0.07 cm^2) emission-extraction system, and run at 21-kV extraction voltage, which yielded I_b = 80- to 90- mA H^- with ±7% current fluctuations as recorded by a 1-MHz BW scope attached to a total beam current Faraday cup located at $z = 3.5$ cm, z being the axial distance from the SAS emission slit. The source discharge ran pulsed with 5-Hz, 1-ms duty factor and H^- beam pulse lengths of 700 μs. The H^- beam current density is j_b = 30 mA/cm^2

* Work supported and funded by the Department of Defense, US Army Strategic Defense Command, under the auspcies of the Department of Energy.

as determined from an emittance scan at $z = 11$ cm. The H^- beam dump (at $z=55$ cm) may be biased. The FGA is located at $z = 22$ cm. Neutralizing gases, in addition to the H_2 gas from the ion source operation (approximately 5×10^{12} cm^{-3}), may be leaked into the transport region. The neutralizing gas density n_g was determined from mass flow meter and Baratron pressure gauge measurements with estimated accuracy of 20–30%. Figure 1 is a schematic representation of the experimental layout. The experiment is done in a rectangular box with typical beam-to-wall distance of 20 cm. The FGA measurements are made several hundred microseconds after the beam pulse start, a time scale long compared to the characteristic neutralization time as noted in Table I.

Results

Positive Ions

The saturated FGA ion current $i_{sat} = i_{FGA}(V_3{=}0)$ is plotted versus $n_g\sigma_i$ in Fig. 3 where σ_i is the ionization cross section of the neutralizing gas by the 21-keV H^- ion (see Table I). Within the detector sensitivity, there is a neutralizing gas density threshold below which no radial positive ion current is observed. This threshold density for He and Xe is listed in Table I and compared with the Gabovich[7] critical density for the assumption that the neutralizing ions are born with 0.1-eV energy, and the agreement is good. In a simple model, if the beam is overneutralized the ions are accelerated radially outward, and the kinetic energy of the ions at the FGA is nearly equal to the plasma potential at their birthplace. If the H^- beam is underneutralized, the ions are trapped in the potential well and no ion current should be observed in the FGA. Positive ions may escape longitudinally to the ion source, beam dump, or a different axial position where radial emission can occur.[8] A prediction for the FGA positive ion current based on the cylindrically symmetric continuity equation at steady state using ionization by the H^- beam as the source term leads to the expression

$$i^+_{FGA} = \frac{r_a^2 T I_b}{2d} \sum_{\substack{\text{all}\\ \text{gases}}} n_g\sigma_i = 486 \sum_{\substack{\text{all}\\ \text{gases}}} n_g\sigma_i \quad (\mu A) \qquad (3)$$

and the predicted current is shown in Fig. 3 as a solid line. Dashed lines are drawn through the data to guide the eye. There is rough agreement with experimental results, particularly for Xe gas, and it is concluded that ionization is the primary source of plasma ions.

Figure 4(A) shows the positive ion energy distribution for $n_{Xe} = 3.5 \times 10^{12}$ cm^{-3}. With the model discussed in the preceding paragraph, the beam potential ϕ_b is given by V_3 at the ion current cutoff, and the width at the base of the ion energy distribution $\Delta\phi$ is the radial potential drop across the beam. Measurements of ϕ_b and $\Delta\phi$ as a function of n_{Xe} are shown in Figs. 5(A) and 5(B). Low ion energies at low neutralizing gas pressures are observed. As the Xe gas density increases, both ϕ_b and $\Delta\phi$ increase to maximum values of about 8 V and 6 V, respectively, for the highest Xe densities measured. These data were acquired over several different days, and the data scatter represents the overall experimental reproducibility.

Helium neutralization gas studies show a slow increase of ϕ_b with He gas density (1 to 2 V) while $\Delta\phi$ is slowly increasing in the 1–2 V range. At high gas densities $\Delta\phi_{Xe} \approx 6$ V and $\Delta\phi_{Xe}/\Delta\phi_{He} \approx 4$, thus favoring Xe as a neutralizing gas because a larger $\Delta\phi$ provides more gas focusing.

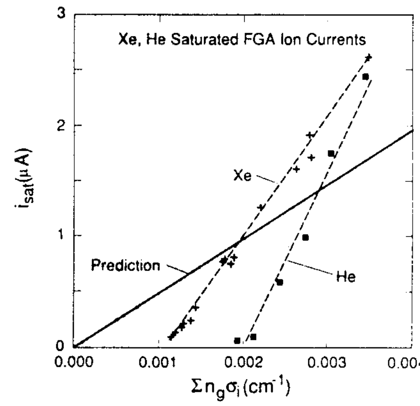

Fig. 3. Saturated positive ion current vs. $n_g\sigma_i$ for He and Xe neutralizing gas. The line is a prediction from Eq. (3) for the FGA current. The $n_g\sigma_i$ value includes H_2 at a density of 5×10^{12} cm^{-3}.

TABLE I. GAS PROPERTIES AND NEUTRALIZATION PARAMETERS FOR NEUTRALIZATION OF 21-keV H^- BEAMS

Gas	σ_i ($\times 10^{-16}$ cm^2)	$\sigma_s = (\sigma_{-10} + \sigma_{-11})$ ($\times 10^{-16}$cm^2)	$n_{Threshold}$ ($\times 10^{12}$cm^{-3})	$n_{Gabovich}$ ($\times 10^{12}$cm^{-3})	$\tau^{(a)}$ (μs)	Transmission$^{(b)}$ (%)
He	0.38	4.8	32.	57	4.1	43
Xe	7.6	40.3	0.53	0.5	12	89
H_2	1.5	9.1				

(a) $\tau = (n_{Threshold}\ \sigma_i\ v_-)^{-1}$
v_- = velocity of H^- beam

(b) Transmission (%) = 100 exp($-\ n_{Threshold}\ \sigma_s\ \ell$)
ℓ = 55 cm, σ_s = H^- beam stripping cross section.

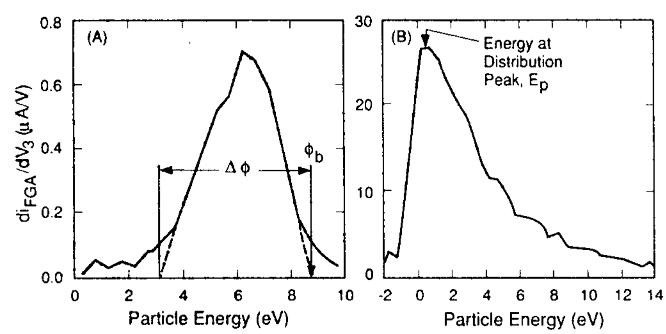

Fig. 4. (A) Positive ion and (B) electron energy distributions taken with $n_{Xe} = 3.5 \times 10^{12}$ cm^{-3}. The quantities ϕ_b and $\Delta\phi$ defined in the text are shown in 5(A), and the peak electron energy is shown in 5(B).

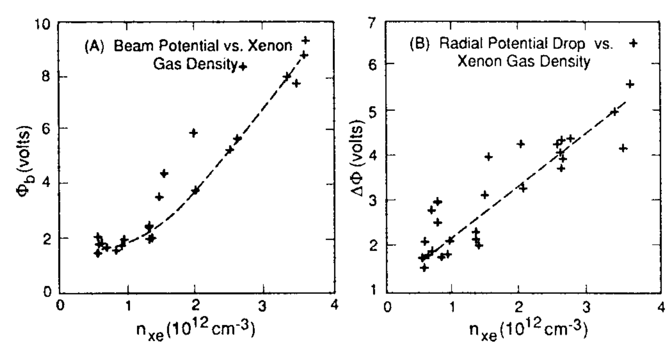

Fig. 5. (A) Beam potential ϕ_b from the positive ion current cutoff on the energy distribution for Xe neutralizing gas. (B) Radial beam potential drop $\Delta\phi$ from the ion distribution width for Xe neutralizing gas. The beam dump is at wall potential in these measurements.

Electrons

The electron saturation current for Xe and He neutralization gases are shown in Fig. 6 versus $n_g\sigma_-$, where $\sigma_- = \sigma_i + \sigma_{-10} + 2\sigma_{-11}$. At low density the electron saturation current scales linearly with the density. At higher density the Xe gas electron current reaches a maximum and then decreases. The He electron current reaches a constant value. The predicted FGA saturation current based on the electron production cross section σ_- is plotted in Fig. 6. Here σ_- replaces σ_i in Eq. (3). There is much larger disagreement between predicted electron currents and experimental results than for the ions, the measurements being an order of magnitude greater than the prediction over most of the density range studied. Some possible explanations are (1) cylindrical symmetry is not correct for the beam/FGA geometry, hence the solid angle calculation given in Eq. (3) would be incorrect; (2) secondary electrons produced on the beam dump, whose current magnitude is 1-2 times greater than that produced by σ_-, are not accounted for in Eq. (3) and (3) there are strong axial dependencies on the radial electron currents, brought about by varying wall distances along the beam transport for instance.

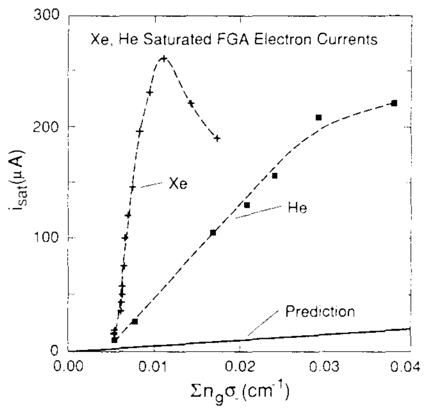

Fig. 6. Saturated electron currents for Xe and He neutralizing gases. The solid line is the electron current predicted by Eq. (3) using σ_- as the source term.

A measured electron energy distribution is shown in Fig. 4(B) for a Xe neutralizing gas density of 3.5×10^{12} cm^{-3}. At low (or zero) Xe gas densities the electron distribution appears to consist of two components, one centered near 10 to 12 eV and having a temperature of 4 to 5 eV and the second peaking near zero energy with $kT_e \approx 2$ eV. The low-energy component may be electrons resulting from ionization of the residual H_2 gas near the FGA entrance by the radially emitted electrons, or an instrumental effect of secondaries produced at the entrance grid. The high-energy component may be electrons accelerated out of the underneutralized beam-plasma region. This component decreases in energy with increasing Xe gas density as shown in Fig. 7(A). The increasing electron current (Fig. 6) is contained in the high-energy component, which coalesces with the low-energy component as it drops in energy. The drop to near-zero energy of the peak of the high-energy component is complete at the threshold Xe density of 5×10^{11} cm^{-3} noted in Table I. The distribution shown in Fig. 4(B) is Maxwellian with temperature $kT_e = 2.6$ eV.

Fig. 7(B) shows the electron temperatures as a function of Xe density. At low densities, the plot of $\ln(i)$ versus V_3 is not linear because the low-energy component is significant, but at

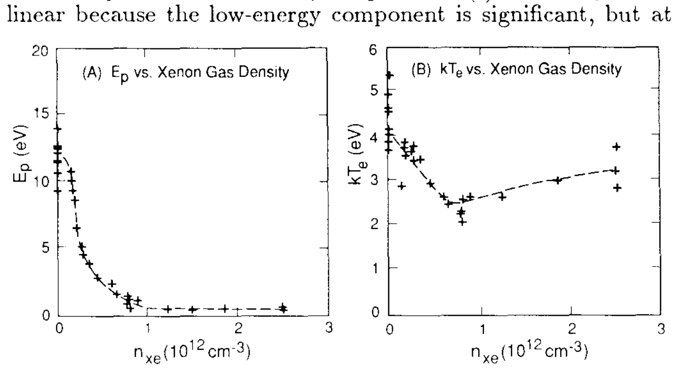

Fig. 7. (A) Electron energy at the distribution maximum and (B) electron temperature vs. Xe density. The beam dump is at wall potential.

higher densities this plot is quite linear. At low densities, kT_e is maximum, drops to a minimum just beyond the critical neutralizing gas density, and then slowly increases with the addition of further Xe gas.

Another feature observed in the FGA electron current is the noise. At zero Xe density, the electron current is very noisy ($\Delta i/i \approx 100\%$), but the percent noise decreases to 10% as the Xe density increases from zero to the threshold density. The percent noise then increases slowly with additional Xe. The noise appears to be broadband over the 1-MHz BW of the current to voltage amplifier. No strong evidence is found for coherent oscillations when the FGA electron signal is analyzed with both a Tektronix 496 Spectrum Analyzer and a fast Fourier transform on data digitized at 32 MHz.

Conclusions

We have developed a gridded energy analyzer for beam neutralization studies of H^- beams, and demonstrated its utility in studying radial currents and energy distributions of both charge polarities. In our experimental setup it was necessary to maintain the analyzer temperature at 350 °C in order to have consistently good (1-eV) energy calibration and resolution. This temperature was found necessary to eliminate nonconducting layers on the grid material. Experiments with 21-keV and 80 to 90-mA H^- beams in Xe and He gas have yielded ion distributions that are consistent with the overneutralization concept of H^- beams. At a certain threshold density for each gas, onset of positive current was observed in the FGA. These densities are close to the Gabovich critical density for H^- beam neutralization. The beam-plasma potential and radial-potential drop across the beam become more positive as the Xe density increases past the threshold density. With no He or Xe neutralization gas present, the measured electron energy distributions are consistent with the beam-plasma potential being approximately −12 V, underneutralized. At the threshold density, Xe is a much more effective gas in preserving the H^- beam current. Beam transmission for the 55-cm transport length at the threshold density shows that 57% of the H^- beam would be stripped using He neutralizing gas, whereas only 11% would be stripped using Xe gas (see Table I).

Acknowledgments

We thank Stuart Orbesen, Patrick Schafstall, and Jim Stelzer for technical assistance in completing these experiments.

References

1. M. D. Gabovich, D. G. Dzhabbarov, and A. P. Naĭda, “Effect of Decompensation of a Dense Beam of Negative Ions,” JETP Lett. **29** (9), 489 (1979).
2. P. W. Allison and J. D. Sherman, “Operating Experience with a 100 keV, 100 mA H^- Injector,” Proc. Third Int. Symp. on the Production and Neutralization of Negative Ions and Beams, Brookhaven National Laboratory, AIP Conf. Proc. **111**, 511 (1983).
3. J. D. Sherman, P. W. Allison, and H. V. Smith, “Beam Potential Measurement of an Intense H^- Beam by Use of the Emissive Probe Technique,” IEEE Trans. Nucl. Sci. **32** (5), 1973 (1985).
4. M. M. Campbell and L. A. Wright, “IVORY PIC Model of Low Energy Beam Transport,” Mission Research Corporation report AMRC-R-969 (1987).
5. A. B. El-Kareh and J. C. J. El-Kareh, *Electron Beams, Lenses, and Optics*, Academic Press, 41 (1970).
6. K. M. Poole, “Electrode Contamination in Electron Optical Systems,” Proc. Phys. Soc. (London) **B66**, 542 (1953).
7. M. D. Gabovich, L. S. Simonenko, and I. A. Soloshenko, “Space-Charge Neutralization of an Intense Negative-Ion Beam,” Sov. Phys. Tech. Phys. **23** (7), 783 (1978).
8. D. G. Dzhabbarov and A. P. Naĭda, “Motion of Positive Ions in the Plasma Produced by a Dense Beam Of Negative Ions in a Gas,” Sov. J. Plasma Phys. **6** (3), 316 (1980).